

Thermal energy storage in rock bed - CFD analysis

Michał Jurczyk^{1✉}, Sebastian Rulik¹, and Łukasz Bartela¹

¹Silesian University of Technology, Poland

✉michal.jurczyk@polsl.pl

Abstract

This article reports on an analysis of the possibility of storing thermal energy in a rock bed. The calculations were made in Ansys CFX 18.0 CFD. The analysis determined the charging time of a packed bed of granite rocks in variable flow conditions for the assumed geometry of the energy storage system. The model was 2-dimensional, consisting of two domains connected by an interface. The packed bed was modelled using a porous model approach. The inlet velocity was varied in the range 0.25–4 m/s. The total charging time was 70 to 1100 min, depending on inlet velocity.

Keywords: thermal energy storage (TES), computational fluid dynamics modeling (CFD), high temperature, rock bed

1 Introduction

Renewable energy sources, such as wind and solar, are taking an increasing share of the energy sector worldwide on the back of climate change concerns. Renewables are used by prosumers to cover their own electricity needs and also constitute a significant percentage of the installed power capacity in energy systems. The growing share of renewables in the energy mix of individual countries may significantly affect the operation of national power grids, leading to suboptimal operation.

As renewable energy sources are characterized by their variable electricity generation, depending on the current weather conditions (wind strength, intensity of solar radiation), a trend of increasing interest in various energy storage technologies can be observed [1, 2, 3]. These technologies include installations using hydrogen as an energy carrier - such as Power to Gas (P2G) and Power to Gas to Power (P2G2P) systems [4, 5, 6] and installations enabling energy storage in the form of compressed air [7, 8].

Issues related to thermal energy storage (TES) are often overlooked in analyses of the energy storage process, although wider use would boost the efficiency of

many installations and help stabilize the operation of energy systems by through their energy savings potential [9]. Currently, TES technologies are widely used in cooperation with solar installations [10, 11]. The implementation of the thermal energy storage systems in buildings may additionally boost building energy efficiency by lowering peak-time needs and decoupling building requirements from energy generation systems [12, 13].

TES processes can be classified into chemical and physical [14, 15], with physical heat storage subdivided into sensible heat storage (SHS) and latent heat storage (LHS). SHS is the simplest and most common form of heat storage. In this process heat is exchanged by a system that changes the temperature of the materials without changing phase. The temperature of the bed is mainly changed by conduction, convection and radiation to absorb (or release) the heat energy. In these solutions change in temperature values in stored materials occurs very slowly. Sensible heat can be described by the formula [14, 16, 17]:

$$Q_h = m \cdot c_p \cdot (\Delta T) = m \cdot c_p \cdot (T_F - T_I) \quad (1)$$

where: Q_h - quantity of the sensible heat storage in a material, c_p - specific heat of the material, m - mass of the material, ΔT - difference between final temperature and initial temperature, T_F - final temperature, T_I - initial temperature.

The article presents an analysis of the possibility of storing thermal energy in a rock bed. A packed bed of granite rocks was used in the calculation model.

2 Calculation algorithm

The presented calculations were performed in Ansys CFX 18.0 CFD. The software uses an implicit finite volume formulation to construct discretized equations representing the unsteady Reynolds-averaged Navier-Stokes (URANS) equations for compressible fluid flow.

Turbulence is modelled using the Rng k-ε turbulence model.

The packed bed is modelled using the porous model approach. The applied porous model is a generalization of the Navier-Stokes equations and of Darcy's law commonly used for flows in porous regions [18]. It can be used to model flows where the geometry is too complex to resolve with a grid. In deriving the continuum equations, it is assumed that infinitesimal control volumes and surfaces are large relative to the interstitial spacing of the porous medium, but small relative to the scales that you want to resolve. Thus, given control cells and control surfaces are assumed to contain both solid and fluid regions [18].

Bed porosity ϵ at a point is the ratio of the volume V' available to flow in an infinitesimal control cell surrounding the point, and the physical volume V of the cell. Hence:

$$V' = \epsilon V \quad (2)$$

It is assumed that the vector area available to flow, A' , through an infinitesimal planar control surface of vector area A is given by:

$$A' = \mathbf{K} \cdot \mathbf{A} \quad (3)$$

Where \mathbf{K} is a symmetric second rank tensor, called the area porosity tensor.

In particular, the equations for conservation of mass 4 and momentum 5 can be presented:

$$\frac{\partial}{\partial t} \epsilon \rho + \nabla \cdot (\rho \mathbf{K} \cdot \mathbf{U}) = 0 \quad (4)$$

$$\begin{aligned} \frac{\partial}{\partial t} (\epsilon \rho \mathbf{U}) + \nabla \cdot (\rho (\mathbf{K} \cdot \mathbf{U}) \otimes \mathbf{U}) - \nabla \cdot \left(u_e \mathbf{K} \cdot (\nabla \mathbf{U} + (\nabla \mathbf{U})^T) - \frac{2}{3} \delta \nabla \cdot \mathbf{U} \right) = \\ = \epsilon \mathbf{S}_m - \epsilon \nabla p \end{aligned} \quad (5)$$

where: \mathbf{U} - true velocity, μ_e - effective viscosity, \mathbf{S}_m - a momentum source (represents resistance to flow in the porous medium).

The momentum loss through an isotropic porous region can be formulated using permeability and loss coefficients as follows:

$$\mathbf{S}_m = -\frac{\mu}{K_{perm}} \mathbf{U} - K_{loss} \frac{1}{2} \rho |\mathbf{U}| \mathbf{U} \quad (6)$$

where: K_{perm} - permeability and K_{loss} - quadratic loss coefficient.

For the assumption that the linear component of this source represents viscous losses and the quadratic term represents inertial losses equations 7 and 8 can be written:

$$C_1 = \frac{\mu}{K_{perm}} \quad (7)$$

$$C_2 = \frac{1}{2} \cdot K_{loss} \quad (8)$$

Both coefficients can be calculated using Ergun's equation according to 9:

$$\begin{aligned} \frac{\Delta p}{L} = \frac{150 \mu (1 - \epsilon)^2}{\epsilon^3 d_p^2} \\ u_s + \frac{1.75 \rho (1 - \epsilon)}{\epsilon^3 d_p} u_s^2 \end{aligned} \quad (9)$$

Superficial velocity u_s in formula 9 is calculated as:

$$u_s = \frac{Q}{A} \quad (10)$$

where: Q - volumetric flow rate through the packed bed, A - total cross-section of the bed

Taking into account Ergun's equation coefficients C_1 , and C_2 can be calculated as:

$$C_1 = \frac{150 \mu (1 - \epsilon)^2}{\epsilon^3 d_p^2} \quad (11)$$

$$C_2 = \frac{1.75 (1 - \epsilon)}{\epsilon^3 d_p} u_s^2 \quad (12)$$

where: C_1 - viscous resistance coefficient, C_2 - inertial resistance coefficient.

The equivalent diameter can be defined as:

$$d_p = \frac{V_p}{S_p} \quad (13)$$

where: V_p - volume of single particle, S_p - surface area of single particle.

For the modelling of heat transfer between the fluid and solid phase a non-thermal equilibrium model

was used. Therefore separate energy equations were solved for the fluid and solid domain according to equations 14 and 15

$$\begin{aligned} \frac{\partial(\varepsilon\rho h)}{\partial t} + \nabla \cdot (\rho\mathbf{K} \cdot \mathbf{U}h) &= \\ &= \nabla \cdot (\lambda_f\mathbf{K}\nabla T) + Q_{fs} \end{aligned} \quad (14)$$

$$\begin{aligned} \frac{\partial((1-\varepsilon)\rho_s\varepsilon h_s)}{\partial t} + \nabla \cdot (\rho\mathbf{K}_s \cdot \mathbf{U}_s h_s) &= \\ &= \nabla \cdot (\lambda_s\mathbf{K}_s\nabla T_s) + Q_{fs} \end{aligned} \quad (15)$$

Where the interfacial heat transfer to the fluid from the solid - Q_{fs} is determined using an overall heat transfer coefficient concept:

$$Q_{fs} = -Q_{sf} = hA_{fs}(T_s - T_f) \quad (16)$$

where: A_{fs} - the interfacial area density between the fluid and the solid, T_f - fluid temperature, T_s - solid temperature.

Interfacial area density between the fluid and the solid describes the amount of total surface area per total volume of porous domain. It can be calculated using porosity and equivalent particle diameter according to formula 17.

$$A_{fs} = \frac{S_{tot}}{V_{tot}} = 6\frac{1-\varepsilon}{d_p} \quad (17)$$

The interstitial convective heat transfer coefficient h is calculated based on the Nusselt number:

$$h = \frac{Nuk_f}{d_p} \quad (18)$$

The Nusselt number is determined according to correlation presented in reference [19] based on particle Reynolds number Re_p and Prandtl number Pr .

$$Nu = 2 + 1.1Re_p^{0.6} + Pr^{\frac{1}{3}} \quad (19)$$

The correlation 20 is valid for $15 < Re_p < 8500$, where Re_p is a particle Reynolds number defined as:

$$Re_p = \frac{\rho u d_p}{\mu} \quad (20)$$

Fig. 1 shows the geometry of the modeled heat accumulator, while Table 1 presents basic assumptions for CFD model and calculation domain. The model is 2-dimensional and consists of two domains connected by an interface. The packed bed is modelled using the porous model approach. The assumed inlet velocity was varied in the range 0.25-4 m/s and the corresponding superficial velocity of packed bed calculated according to relation 9 was in the range 0.125-2 m/s.

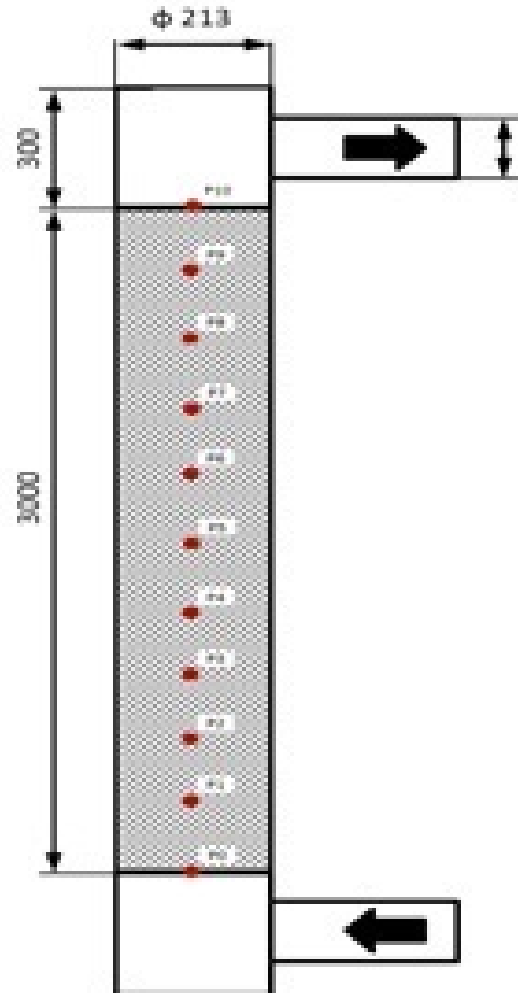


Figure 1: Geometry of the modeled heat accumulator

The porous domain consists of granite and air. Basic assumptions for the porous domain are listed in Table 2. Permeability and loss coefficients are calculated based on formulas 7-13. It was assumed that the

Table 1: Calculation domain and basic assumptions for the applied CFD model

Boundary conditions	
Inlet velocity	0.25 m/s, 1.0 m/s, 4.0 m/s
Inlet temperature	200 °C
Outlet:	0 Pa
External walls:	no-slip, adiabatic
Properties of fluid and solid domain	
Property	Air
Density, kg/m^3	According to perfect gas law
Specific heat, J/kgK	1004.4
Thermal conductivity, W/mK	0.0244
Property	Granite
Density, kg/m^3	2600
Specific heat, J/kgK	790
Thermal conductivity, W/mK	3.1

Table 2: Porous domain details

Particle diameter	2 cm
Porosity	0.4
Interfacial area density	$180 m^{-1}$
Permeability coefficient	$4.74 \cdot 10^{-7} m^2$
Loss coefficient	$1640.6 m^{-1}$
Heat transfer coefficient	21-98 $W(m^2K)$

equivalent diameter of granite particles was 2 cm and the porosity of the whole packed bed was 0.4. The interfacial area density calculated according to 17 was $180 m^{-1}$. The heat transfer coefficient was determined according to formulas 18-20. Depending on the flow velocity, its value varied in the range 21 -98 $W(m^2K)$.

The properties of air, including thermal conductivity and viscosity, were temperature dependent. Sutherland’s formula was incorporated in both cases. The temperature along the packed bed was monitored in 11 equally spaced locations. Hexa type mesh was used for the analysis, including 40 000 nodes. The time step of transient analysis was set at 5 s. The initial conditions reflect ambient conditions, with a temperature of 20 °C.

3 Calculation results

The main purpose of the analysis was to determine the charging time of a packed bed of granite rocks in variable flow conditions. The geometry and parameters of packed bed were fixed, as listed in Table 2. The results obtained concern three different inlet velocities of 0.25 m/s, 1.0 m/s and 4.0 m/s. The calculated particle Reynolds number lay within a wide range of 120-1910.

The heat transfer coefficient calculated based on relation 18 and 19 was 21 $W(m^2K)$, 44 $W(m^2K)$ and 98 $W(m^2K)$ respectively. Additionally, the pressure drop along the packed bed was determined for each investigated case.

Figures 2-4 presents the temperature distribution of air and granite for 6 locations along the center line of the packed bed as a function of time during the charging process for variable flow conditions. The distribution of monitor points is given in Fig. 1.

The total charging time varies between 70 to 1100 min depending on the assumed inlet velocity. Decreasing the inlet velocity leads to smaller differences between the solid rock particles and flowing air, and low Nusselt numbers. Both of these factors lead to a major extension of the time required to heat the whole packed bed of rocks.

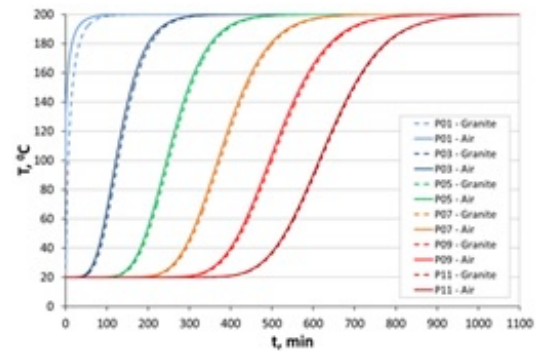


Figure 2: Temperature distribution of air and granite for different points located along the packed bed during the charging process, $u_{in}=0.25 m/s$, $u_s=0.125 m/s$

Fig. 5 shows temperature distribution along the whole tank and packed bed for inlet velocity of 1 m/s. A large temperature gradient is visible along the packed bed height in case of initial phase. This means that majority of heat is transferred directly to the cold packed bed and the outlet temperature from the tank is relatively low. The outlet temperature exceeds 50 °C after about 120 minutes of charging.

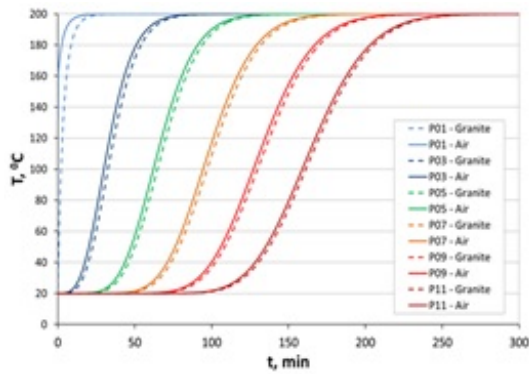


Figure 3: Temperature distribution of air and granite for different points located along the packed bed during the charging process, $u_{in}=1$ m/s, $u_s=0.5$ m/s

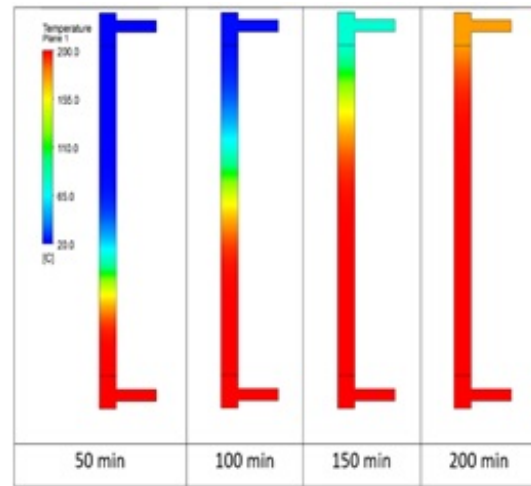


Figure 5: Temperature distribution of air in the heated packed bed, $u_{in}=1$ m/s

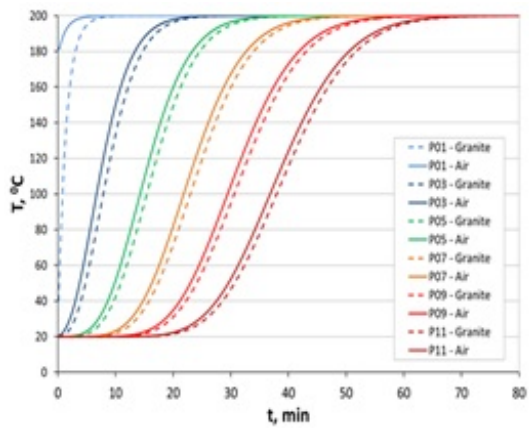


Figure 4: Temperature distribution of air and granite for different points located along the packed bed during the charging process, $u_{in}=4$ m/s, $u_s=2.0$ m/s

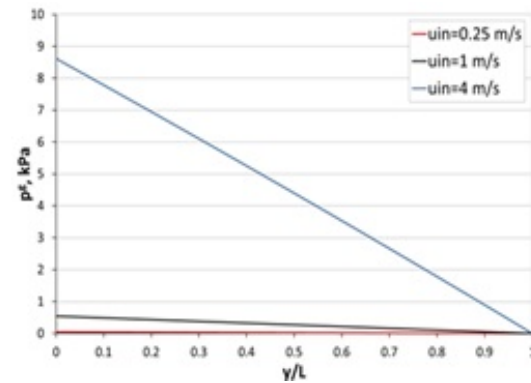


Figure 6: Distribution of normalized velocity vectors, $u_{in}=1$ m/s, $u_s=0.5$ m/s

Figure 6 shows the distribution of gauge pressure along the packed bed for three investigated inlet velocities. The pressure drop for inlet velocity of 0.25 m/s was only 47 Pa. For velocity of 1 m/s it was 544 Pa while for velocity of 4 m/s it reached 8630 Pa. In each case the pressure drop along the packed bed is almost linear.

Fig. 7 presents the distribution of normalized velocity vectors for the fully charged packed bed for the same flow conditions. One large vortex is visible in the inlet section to the packed bed. A significant acceleration of the flow can be observed along the packed bed due to its porosity. The velocity along the packed bed is uniform. However, in the case of high temperature gradients in the initial phase of charging, the velocity along the packed bed falls due to the temperature drop and related increase in air density.

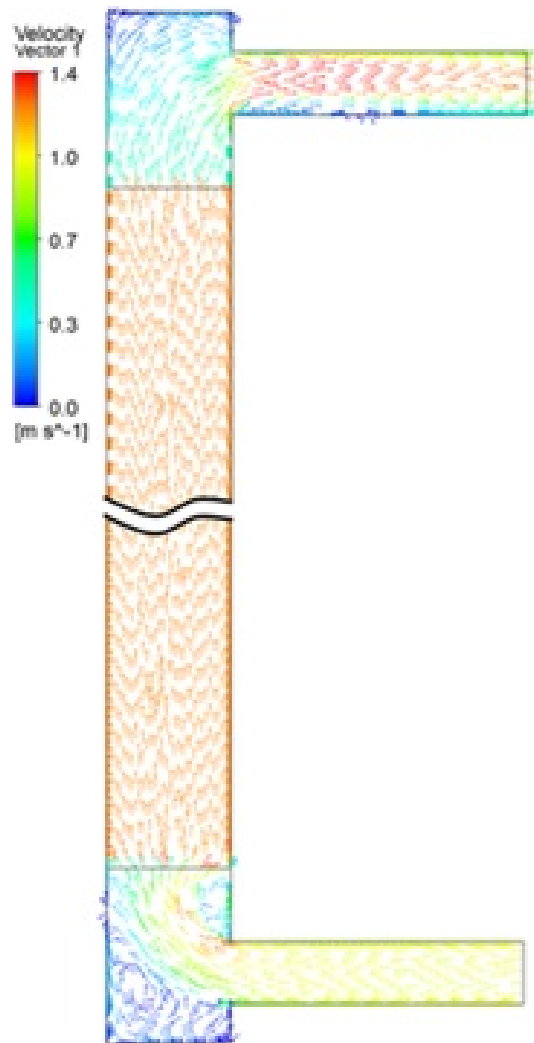


Figure 7: Distribution of pressure drop along the normalized packed bed length

4 Summary/Conclusions

The main purpose of this work was to analyze the possibility of storing thermal energy in a rock bed. A packed bed of granite rocks was used in the calculation model. The main purpose of the calculations was to determine the charging time of the packed bed in variable flow conditions.

The results obtained concern three different inlet velocities of 0.25 m/s, 1.0 m/s and 4.0 m/s. The total charging time varies between 70 and 1100 min depending on the assumed inlet velocity. Decreasing the inlet velocity leads to smaller differences between the solid rock particles and flowing air, and low Nusselt numbers. Both of these factors lead to a very significant extension of the time needed to heat the whole packed bed of rocks.

For inlet velocity of 1 m/s the outlet temperature exceeds 50°C after about 120 minutes of charging. For three investigated inlet velocities, the distribution of gauge pressure along the packed bed was investigated. The pressure drop for inlet velocity of 0.25 m/s was the smallest (47 Pa) whereas for velocity of 4 m/s the pressure drop reached its highest value of 8630 Pa.

The next stage of research is to construct a test stand and dedicated measuring system for the purpose of detailed studies and verification of the results from the numerical model reported in this paper.

5 Acknowledgements

Publication supported by Own Scholarship Fund of the Silesian University of Technology in 2019/2020.

References

- [1] Wojciech Uchman, Anna Skorek-Osikowska, Michał Jurczyk, and Daniel Wecel. The analysis of dynamic operation of power-to-SNG system with hydrogen generator powered with renewable energy, hydrogen storage and methanation unit. *Energy*, 213, 2020.
- [2] Łukasz Bartela. A hybrid energy storage system using compressed air and hydrogen as the energy carrier. *Energy*, 196, 2020.
- [3] Janusz Kotowicz, Łukasz Bartela, Daniel Wecel, and Klaudia Dubiel. Hydrogen generator characteristic for storage of renewably-generated energy. *Energy*, 118:156–171, 2017.
- [4] Janusz Kotowicz, Daniel Wecel, and Michał Jurczyk. Analysis of component operation in Power to Gas to Power operation. *Applied Energy*, 216:45–59, 2018.
- [5] Jakub Kupecki, Konrad Motylinski, Stanisław Jagielski, Michał Wierzbicki, Jack Brouwer, Yevgeniy Naumovich, and Marek Skrzypkiewicz. Energy analysis of a 10 kW-class power-to-gas system based on a solid oxide electrolyzer (SOE). *Energy Conversion and Management*, 199, 2019.
- [6] Linda Barelli, Gianni Bidini, Giovanni Cinti, and Jarosław Milewski. High temperature electrolysis using Molten Carbonate Electrolyzer. *International Journal of Hydrogen Energy*, Article in Press, 2020.
- [7] Jarosław Milewski, Krzysztof Badyda, and Łukasz Szabłowski. Compressed Air Energy

- Storage Systems. *Journal of Power Technologies*, 96:245–260, 2016.
- [8] Marlena Wróbel and Jacek Kalina. Preliminary evaluation of CAES system concept with partial oxidation gas turbine technology. *Energy*, 183, 2019.
- [9] Pablo Arce, Marc Medrano, Antoni Gil, Eduard Oró, and Luisa F. Cabeza. Overview of thermal energy storage (TES) potential energy savings and climate change mitigation in Spain and Europe. *Applied Energy*, 88:2764–2774, 2011.
- [10] Vivek R. Pawar and Sarvenaz Sobhansarbandi. CFD modeling of a thermal energy storage based heat pipe evacuated tube solar collector. *Journal of Energy Storage*, 30, 2020.
- [11] Burcu Koçak, Ana Ines Fernandez, and Halime Paksoy. Review on sensible thermal energy storage for industrial solar applications and sustainability aspects. *Solar Energy*, 2020.
- [12] MCarmen Guerrero Delgado, José Sánchez Ramos, Servando Álvarez Domínguez, José Antonio Tenorio Ríos, and Luisa F. Cabeza. Building thermal storage technology: Compensating renewable energy fluctuations. *Journal of Energy Storage*, 27, 2020.
- [13] Michal Pomianowski, Per Heiselberg, and Yinping Zhang. Review of thermal energy storage technologies based on PCM application in buildings. *Energy and Buildings*, 67:56–69, 2013.
- [14] Hussam Jouhara, Alina Żabnieńska Góra, Navid Khordehgah, Darem Ahmad, and Tom Lipinski. Latent thermal energy storage technologies and applications: A review. *International Journal of Thermofluids*, 5-6, 2020.
- [15] S. Koochi-Fayegh and M.A. Rosen. A review of energy storage types, applications and recent developments. *Journal of Energy Storage*, 27, 2020.
- [16] Pushpendra Kumar Singh Rathore, Shailendra Kumar Shukla, and Naveen Kumar Gupta. Potential of microencapsulated PCM for energy savings in buildings: A critical review. *Sustainable Cities and Society*, 53, 2020.
- [17] Pushpendra Kumar Singh Rathore and Shailendra Kumar Shukla. Potential of macroencapsulated PCM for thermal energy storage in buildings: A comprehensive review. *Construction and Building Materials*, 225:723–744, 2019.
- [18] CFX Manual. 2020.
- [19] N. Wakao, S. Kagueli, and T. Funazkri. Effect of fluid dispersion coefficients on particle-to-fluid heat transfer coefficients in packed beds: Correlation of nusselt numbers. *Chemical Engineering Science*, 34:325–336, 1979.